

## Antisymmetric magnetoresistance and helical magnetic structure in a compensated Gd/Co multilayer

Surendra Singh,<sup>1,2,\*</sup> M. A. Basha,<sup>1,2</sup> C. L. Prajapat,<sup>2,3</sup> Harsh Bhatt,<sup>1</sup> Yogesh Kumar,<sup>1</sup> M. Gupta,<sup>4</sup> C. J. Kinane,<sup>5</sup> J. Cooper,<sup>5</sup> M. R. Gonal,<sup>6</sup> S. Langridge,<sup>5</sup> and S. Basu<sup>1,2</sup>

<sup>1</sup>*Solid State Physics Division, Bhabha Atomic Research Centre, Mumbai 400085, India*

<sup>2</sup>*Homi Bhabha National Institute, Anushaktinagar, Mumbai 400094, India*

<sup>3</sup>*Technical Physics Division, Bhabha Atomic Research Centre, Mumbai 400085, India*

<sup>4</sup>*UGC DAE Consortium for Scientific Research, University Campus, Khandwa Road, Indore 452017, India*

<sup>5</sup>*ISIS-STFC, Rutherford Appleton Laboratory, Didcot OX11 0QX, United Kingdom*

<sup>6</sup>*Glass and Advanced Material Division, Bhabha Atomic Research Centre, Mumbai 400085, India*



(Received 8 April 2019; revised manuscript received 5 September 2019; published 11 October 2019)

Using spin-dependent specular and off-specular polarized neutron reflectivity (PNR), we report the observation of a twisted helical magnetic structure with planar  $2\pi$  domain walls (DWs) and highly correlated magnetic domains in a Gd/Co multilayer. Specular PNR with a polarization analysis reveals the formation of planar  $2\pi$  DWs below a compensation temperature ( $T_{\text{comp}}$ ), resulting in a negative exchange bias in this system. Off-specular PNR with spin polarization showed the development of magnetic inhomogeneities (increase in magnetic roughness) for the central part (thickness  $\sim 25\text{--}30$  Å) of each Gd layer, where magnetization is aligned perpendicular (in plane) to an applied field. This is contributing towards an antisymmetric magnetoresistance at  $T_{\text{comp}}$  in the system. The magnetic roughness is vertically correlated and results in a Bragg sheet observed in the spin-flip channel of off-specular PNR data. The growth and tunability of highly correlated magnetic inhomogeneities (roughness) and the domain structure around  $T_{\text{comp}}$  in a combination of a twisted helical magnetic structure with planar  $2\pi$  DWs will be key for applications in all-spin-based technology.

DOI: [10.1103/PhysRevB.100.140405](https://doi.org/10.1103/PhysRevB.100.140405)

### I. INTRODUCTION

The current-induced manipulation of magnetic order through a spin-orbit torque has recently attracted great interest for the realization of magnetic memory and logic application devices with fast switching [1–5]. The Dzyaloshinskii-Moriya interaction [6], and the spin Hall effect via heavy-metal layers [7–9] were the major phenomena that attributed to large chiral spin torques. An exchange coupling torque (ECT) recently showed a significant enhancement of the spin-torque efficiency in artificial antiferromagnetic (AF) structures [10,11], which allows moving nanoscale magnetic domain walls (DWs) with the current at large velocities [10].

The compensated rare earth (RE)–transition metal (TM) alloys and heterostructures, where the RE and TM moments are aligned antiparallel due to the strong AF interaction and the net moment tends to zero, are potential candidate materials for realizing devices with higher speed and density [12–16]. A class of ferrimagnets consisting of RE-TM alloys and heterostructures also has the potential to exhibit DW motion via an ECT [17,18]. Fast switching in compensated systems can further be influenced by magnetic [16,19] and optical [20] fields. Recently, Vedmedenko *et al.* [21] have pointed out theoretically that nanosized stable magnetic helices can be used for magnetic energy storage. The realization of magnetic

helices with stable magnetic properties has also been studied theoretically [22] and experimentally [23] in exchange-coupled thin films and RE/TM multilayers, respectively. It is recognized that magnetization reversal and a magnetic helical configuration (planar  $2\pi$  DWs) in RE-TM multilayers with no external magnetic field around the compensation temperature ( $T_{\text{comp}}$ , the temperature at which total moments of the RE-TM multilayer tend to zero) is the key to manipulating magnetic devices [20,23]. However, the response of interface DWs in RE-TM heterostructures across the  $T_{\text{comp}}$  to magnetic fields and/or electric currents depends on the magnetic structure, magnetic phases, and domain evolution at the interfaces.

Here, we present strong evidence of helices in the form of planar  $2\pi$  DWs within both layers of Gd and Co in Gd/Co multilayers near the  $T_{\text{comp}}$  using polarized neutron reflectivity (PNR) [24–28]. PNR confirms an AF coupling between the Gd and Co layers. AF coupling along with the planar  $2\pi$  DW formation in this multilayer below  $T_{\text{comp}}$  is responsible for the observed negative exchange bias. We also observed antisymmetric magnetoresistance (MR) at  $T_{\text{comp}}$ , which is in contrast to earlier findings of similar effects in magnetic heterostructures with perpendicular magnetic anisotropy. Using spin-dependent specular and off-specular PNR we demonstrate that antisymmetric MR at  $T_{\text{comp}}$  is a result of the evolution of highly correlated magnetic inhomogeneities (roughness) and magnetic domains of submicron length scale, in which the magnetization is aligned perpendicular (in plane) to the applied field.

\*surendra@barc.gov.in

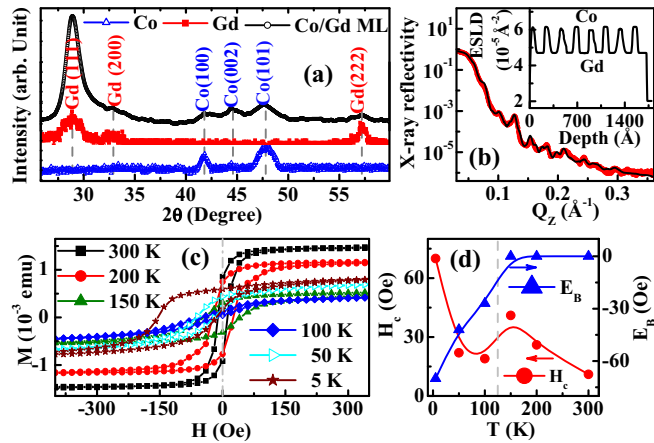


FIG. 1. (a) XRD scan for the Gd/Co multilayer, and single Co and Gd films. (b) XRR data from the multilayer. The inset shows the ESLD depth profile extracted from XRR data. (c) The in-plane DC magnetization [ $M(H)$ ] curve at different temperatures. (d) Variation of coercive field ( $H_c$ ) and exchange bias ( $E_B$ ) as a function of temperatures.

## II. RESULTS AND DISCUSSION

The Gd/Co multilayer was grown using dc magnetron sputtering [29] on a Si (100) substrate (see Supplemental Material [30]) with a nominal structure Si/[Gd(140 Å)/Co(70 Å)] $\times$ 8, where 8 is the number of repeats. Figure 1(a) shows the x-ray diffraction (XRD) patterns recorded for the Gd/Co multilayer along with single Co and Gd films. In contrast to earlier studies on Gd/Co multilayer systems [31,32], where an hcp structure for the Gd layer was observed, we found that the Gd layer has grown with a polycrystalline fcc structure [33]. However, Co has grown with a polycrystalline hcp structure. These results are consistent with an earlier study on Gd/Co multilayers grown on glass substrates [34]. Figure 1(b) shows the x-ray reflectivity (XRR) data for the multilayer. Analysis of the XRR data provides the individual layer thickness, electron scattering length density (ESLD), and root mean square (rms) roughness at different interfaces of the multilayer [25,26,35–37]. The inset of Fig. 1(b) shows the ESLD depth profile of the multilayer extracted from the XRR data. Parameters obtained from XRR are given in Table S1 [30]. Small variations in the roughness of each interface were considered to get the best fit for the XRR data. XRR results are corroborated by secondary-ion mass spectrometry measurements (Fig. S1 [30]).

Figure 1(c) shows the in-plane magnetic hysteresis curves for the multilayer at different temperatures measured by a superconducting quantum interference device (SQUID) magnetometer. The observation of a very small coercive field ( $H_c \approx 15$  Oe) at 300 K, where only the Co is ferromagnetic, indicates the soft ferromagnetic nature of the multilayer. Magnetization data at different temperatures reveal a reduction in the saturation magnetization, an increase in  $H_c$ , and a shift of the hysteresis loop to the negative magnetic field ( $H$ ) at low temperatures [Fig. 1(c) and Fig. S2 [30]]. The shift of the hysteresis loop to the negative field at low temperature reveals the negative exchange bias ( $E_B$ ) in the multilayer. Figure 1(d) shows the variation of  $H_c$  and  $E_B$  with

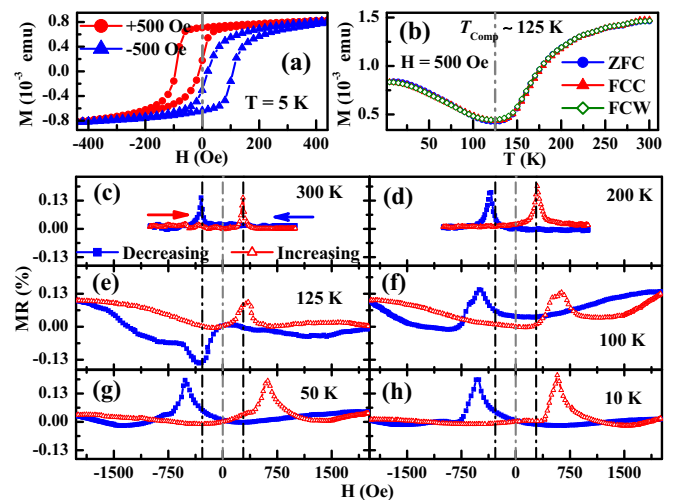


FIG. 2. (a)  $M(H)$  curves at 5 K on FC the sample at  $\pm 500$  Oe. (b) Magnetization data as a function of temperature from multilayers for ZFC, FCC, and FCW conditions. (c)–(h) MR (%) data for the multilayer at different temperatures. The magnetic field is applied along the plane of the multilayer during  $M(H)$  and MR measurements.

temperature. We observed the shift of the magnetic hysteresis loop below  $\sim 150$  K ( $E_B$  increases below this temperature), where  $H_c$  starts decreasing.

The exchange bias at 5 K was further confirmed by measuring the in-plane magnetic hysteresis loops [Fig. 2(a)] of the multilayer after field cooling (FC) from room temperature in an applied  $H$  of  $\sim \pm 500$  Oe. A shift of the hysteresis loop along the  $H$  axis was observed towards negative (positive) fields on cooling the sample in a field of + (–)500 Oe, confirming the negative  $E_B$  in the system. Figure 2(b) shows the  $M(T)$  data from the multilayer under FC [cooling (FCC) and warming (FCW) cycle] and zero-field-cooled (ZFC) conditions in an in-plane  $H$  of 500 Oe, showing an identical variation as a function of temperature. The  $M(T)$  data for the multilayer show a minimum in magnetization at a temperature around 125 K ( $\sim T_{\text{comp}}$ ).

Figures 2(c)–2(h) show the magnetoresistance (MR) data (%) [ $= \frac{[\mathcal{R}(H) - \mathcal{R}(0)]}{\mathcal{R}(0)} \times 100$ , where  $\mathcal{R}(H)$  and  $\mathcal{R}(0)$  are the resistances in the magnetic field  $H$  and in zero field] at different temperatures in the longitudinal direction ( $H$  and the current are in the same direction and along the plane of the film) as a function of the  $H$ . MR data measured on sweeping the  $H$  in the positive and negative direction are represented by red (line with open triangles) and blue (line with solid squares) curves, respectively. We observed different MR data as a function of temperature. The  $H$  dependences of the MR data at 300 and 200 K show almost reversible (saturated) regions beyond the resistance peaks, similar to other magnetic multilayers. However, the resistance peaks are observed at fields much higher than the coercive field [Fig. 2 and Fig. S3 [30]], which might be due to strong interface scattering in the system [30,38–40]. We obtained irreversible and antisymmetric MR at 125 K. The MR data at 100 K and below again show the symmetric MR peaks. Although we observed additional irreversibility (separation) in the MR data when the  $H$  is scanned in opposite directions, irreversibility

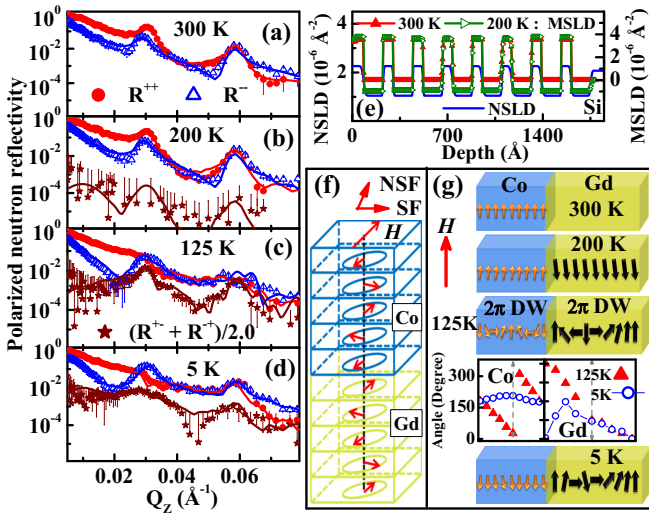


FIG. 3. (a)–(d) PNR data [NSF:  $R^{++}$  (red  $\bullet$ ),  $R^{-}$  (blue  $\Delta$ ); SF:  $(R^{++} + R^{-})/2.0$  (maroon  $*$ ) and corresponding fits (solid lines) from the Gd/Co multilayer at different temperatures under an applied in-plane field ( $H$ ) of 500 Oe. (e) Nuclear and magnetic scattering length density (NSLD and MSLD) depth profiles of the multilayer. (f) Schematic of the helical magnetic structure. (g) Representation of magnetization in a bilayer of a Gd/Co multilayer obtained from PNR data at different temperatures. The angle of rotation of the magnetization with respect to the  $H$  in different sublayers within the Gd and Co layers at 125 and 5 K.

in the MR beyond the peak region for different  $H$  directions decreases on decreasing the temperature. Similar changes in the resistance at the low magnetic field for temperatures other than 125 K have been reported previously for Fe/Gd [41–43] and Co/Gd [44] systems.

In order to understand the correlation of the macroscopic magnetization (SQUID) and MR properties of the multilayer, we have studied the depth-dependent structure and magnetization using PNR at different temperatures. PNR measurements (Fig. S4 [30]) were carried out using the OFFSPEC reflectometer (wavelength range 2.2–14  $\text{\AA}$ ) at RAL, U.K. PNR data were taken in the  $H$  of +500 Oe at different temperatures upon warming, after the sample was cooled at the same field from 300 to 5 K. Specular ( $Q_x = 0$ ) PNR with a polarization analysis, i.e., non-spin-flip (NSF),  $R^{++}$  and  $R^{-}$ , and spin-flip (SF),  $R^{++}$  and  $R^{-}$ , reflectivities, are used to determine the magnitude and direction of the magnetization vector along the depth of the multilayer [45–47]. For these measurements, NSF probes the projection of the magnetic induction vector parallel to the polarization direction, while SF is sensitive to the perpendicular component [Fig. 3(f)]. Figures 3(a)–3(d) show the  $R^{++}$  (red solid circle),  $R^{-}$  (blue open triangle), and  $(R^{++} + R^{-})/2.0$  (maroon asterisk) reflectivity and corresponding fits (continuous lines) as a function of the wave-vector transfer  $Q_z$ , normal to the sample surface, at different temperatures. The specular reflectivity data are collected up to a  $Q_z$  of  $\sim 0.08 \text{\AA}^{-1}$ , which includes two Bragg peaks (BP) at  $Q_z \sim 0.03 \text{\AA}^{-1}$  (first order) and  $0.06 \text{\AA}^{-1}$  (second order) which corresponds to a bilayer periodicity of  $\sim 212 \text{\AA}$ . Figure 3(e) shows the nuclear scattering length density

(NSLD) depth profile of the multilayer obtained from the specular PNR, which is consistent with the ESLD profile obtained from XRR data.

It is noteworthy that Gd exhibits a large absorption for thermal neutron [48]. PNR data with [Fig. 3(a)] and without (PNR data up to a larger  $Q_z \sim 0.16 \text{\AA}^{-1}$ , Fig. S6 [30]) a polarization analysis were used to fit the  $\rho_N$  for Gd. We obtained  $\rho_N = (1.05 + i3.42) \times 10^{-6} \text{\AA}^{-2}$  for Gd, which is very close to  $(0.96 + i3.12) \times 10^{-6} \text{\AA}^{-2}$  for a neutron of wavelength 2.6  $\text{\AA}$  [48]. The strong AF interaction in this system persists even for thicker Gd ( $\sim 140 \text{\AA}$ ) and Co ( $\sim 70 \text{\AA}$ ) layers, which may be due to the large exchange coupling ( $J_{AF} = -2.1 \times 10^{-15}$  ergs) [31] between Co and Gd spins as compared to the Zeeman energy ( $\mu_B H = 4.6 \times 10^{-18}$  ergs for  $H = 0.5$  kOe, field applied to the sample for the PNR measurements).

We did not observe any SF [ $(R^{++} + R^{-})/2.0$ ] signal at 300 K [Fig. 3(a)], suggesting ferromagnetic Co with a magnetic scattering length density (MSLD) of  $\sim (3.55 \pm 0.16) \times 10^{-6} \text{\AA}^{-2}$  ( $\sim 1.52 \mu_B/\text{atom}$ ) and zero MSLD for the Gd layer. At 200 K we observed AF coupling between the Gd and Co layer, where the Co moments (MSLD  $\sim 3.78 \pm 0.17 \times 10^{-6} \text{\AA}^{-2} \sim 1.65 \mu_B/\text{atom}$ ) are aligned along the direction of the  $H$  and the Gd moments (MSLD  $\sim -0.85 \pm 0.05 \times 10^{-6} \text{\AA}^{-2} \sim -1.40 \mu_B/\text{atom}$ ) are aligned antiparallel. The MSLD depth profiles at 300 and 200 K are shown in Fig. 3(e). For comparison, negligible SF reflectivity is observed at 200 K. The solid line fit [Fig. 3(b)] for SF data at 200 K assumes a small inclination of the moments from the applied field by a small angle ( $\sim 1^\circ$ – $1.5^\circ$ ), suggesting the moments are essentially parallel to applied field at 200 K within error.

Strong SF signals are observed in the specular PNR data at 125 and 5 K. Figure 3(c) clearly suggests additional modulation in the PNR data at these low temperatures, e.g., a decrease in the intensity of  $R^{++}$  data around the first-order BP and splitting of second-order BP for  $R^{++}$  (for 125 K), suggesting a modification in the magnetic structure. Attempts to fit the PNR data at 125 and 5 K with homogeneous Gd and Co layers failed to reproduce the observed results and thus we considered a helical magnetic structure as depicted in Fig. 3(f), similar to the Dy/Fe multilayer [23]. We have split the individual Co and Gd layers into sublayers with a constant magnetic moment within the Co and Gd layers but varying the angle of rotation of the magnetization with respect to the  $H$ , i.e., a helical structure. PNR data at 125 K reveal that the magnetization in both the Gd and Co layers rotate by  $2\pi$  and form a planar  $2\pi$  DW structure [23] as shown in Fig. 3(g). However, at the interfaces, Gd and Co have coupled antiferromagnetically, where Gd (Co) is aligned along (opposite) the  $H$ , which is consistent with the earlier findings for the RE-TM system [49]. We have plotted the observed magnetization rotation angle in Fig. 3(g) for the sublayers within the Co and Gd layer, suggesting asymmetric rotation along the thickness of the Gd layer (i.e., the magnetization of the central part of the Gd layer is rotated by  $90^\circ$  instead of  $180^\circ$  as in the case of the Co layer). Therefore the depth-dependent magnetic structure of the multilayer at  $T_{\text{comp}}$  exhibits the twisted helical structure. PNR measurements at 5 K suggested that the Co

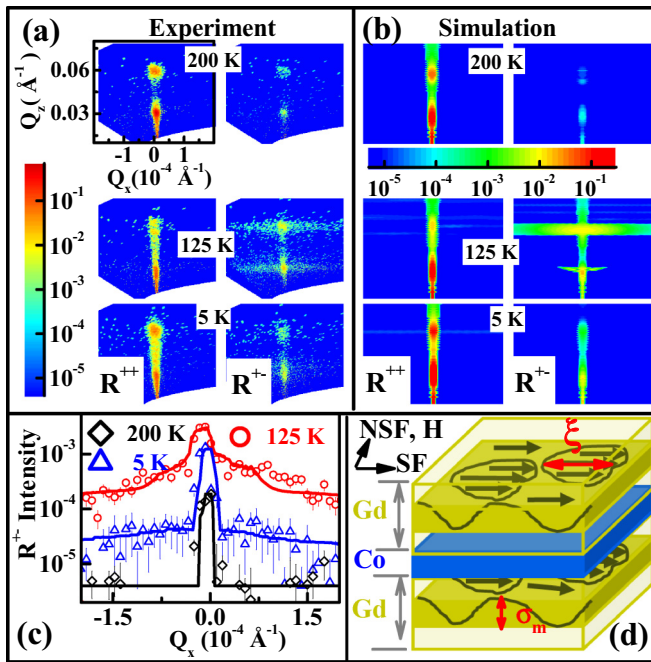


FIG. 4. (a) Off-specular PNR data ( $Q_x - Q_z$  map) from the Gd/Co multilayer at different temperatures in NSF ( $R^{++}$ ) and SF ( $R^{+-}$ ) modes under an applied in-plane field ( $H$ ) of 500 Oe. (b) Simulated profiles at different temperatures. (c)  $R^{+-}$  intensity (scattered) and fit (continuous line) around the  $Q_z \sim 0.06 \text{ \AA}^{-1}$  at different temperatures. (d) Schematic of spin alignment of the Gd layer in a bilayer, contributing to the Bragg sheet in  $R^{+-}$  intensity at 125 K.

magnetization is still aligned opposite to the  $H$  with a small variation in angle ( $180^\circ \pm 10^\circ$ ) for the Co sublayers, while the magnetization of the Gd sublayer forms a  $2\pi$  rotation within the Gd layer, which follows the  $0-\pi-0$  rotation, instead of the full  $2\pi$  ( $0$  to  $2\pi$ ), as shown in Fig. 3(g).

While specular PNR as a function of  $Q_z$  provides depth profiles of the nuclear and magnetic structures, the lateral wave-vector transfer  $Q_x$  provides information on the correlation of lateral magnetic inhomogeneities (roughness and domains) in the sample plane, via off-specular scattering [30,50–52]. Figure 4(a) depicts the off-specular NSF ( $R^{++}$  and  $R^{+-}$ ) data ( $Q_x - Q_z$  intensity map) at 5, 125, and 200 K. The  $Q_x - Q_z$  intensity map for  $R^{++}$  did not show any off-specular signals at different temperatures. However, we obtained strong off-specular signals (Bragg sheet: intensity along  $Q_x$  at Bragg positions) for the SF ( $R^{+-}$ ) mode at 125 K, which disappeared at high (200 K) as well as low (5 K) temperatures and hence suggesting a magnetic origin. Bragg sheets in the  $R^{+-}$  reflectivity map at 125 K ( $= T_{\text{comp}}$ ), clearly indicate the development of magnetic inhomogeneities at interfaces that are vertically correlated. Variations of the SF off-specular intensity (scattered) and corresponding fit (solid lines) at the second BP ( $Q_z \sim 0.06 \text{ \AA}^{-1}$ ) as a function of  $Q_x$  for different temperatures are also compared in Fig. 4(c), justifying a magnetic source of the scattering at 125 K. Figure 4(b) shows the corresponding simulated  $R^{++}$  and  $R^{+-}$  map at different temperatures. Simulation of the off-specular reflectivity has been performed using the distorted wave Born approximation [30,51,52]. Bragg sheets in the SF off-specular

map at 125 K are well described by an in-plane correlation length (magnetic domains) ( $\sim \xi$ ) of  $0.17 \text{ \mu m}$  at the central part [thickness  $\sim 25\text{--}30 \text{ \AA}$  with an rms magnetic roughness ( $\sigma_m$ )  $\sim 9 \text{ \AA}$ ] in each Gd layer in the multilayer, for which the magnetic moment is aligned perpendicular (in plane) to the  $H$ , as shown in Fig. 4(d) for a bilayer. We observed a fivefold increase in  $\sigma_m$  for these interfaces at 125 K [30], as compared to that of 200 and 300 K. Moreover,  $\sigma_m$  for these intermediate Gd layers at 125 K is vertically correlated. We found smaller  $\xi$  ( $\sim 0.01 \text{ \mu m}$ ) for all the interfaces below and above 125 K. The absence of a Bragg sheet at 5 K indicates the development of uncorrelated roughness.

AF coupling of RE-TM systems has been attributed to the formation of planar DWs ( $2\pi$  DW) at the interfaces [53]. These  $2\pi$  DWs were responsible for the origin of  $E_B$  in RE-TM multilayers [54,55]. Our results for Gd/Co multilayers are consistent with these findings as we observed  $E_B$  developing in the system near  $T_{\text{comp}}$ , where there is a strong AF coupling between Gd and Co and specular PNR clearly suggested the formation of magnetic helices with  $2\pi$  DWs within each Gd and Co layer. The  $E_B$  increases at low temperature and we obtained the highest  $E_B$  of  $\sim -75$  Oe at 5 K. At 5 K, Co moments are mostly aligned opposite to the applied field and the interface Gd moments are aligned opposite (aligned along  $H$ ) to Co moments, while the moments in Gd layers form twisted helices with a  $0-\pi-0$  configuration of the magnetization.

Another remarkable finding is the antisymmetric MR at  $T_{\text{comp}}$  and irreversibility in MR as a function of the  $H$  around  $T_{\text{comp}}$ . Different mechanisms are proposed to understand the MR effects in magnetic materials, however, these effects share a common symmetry with respect to magnetization reversal, namely,  $\text{MR}(H) = \text{MR}(-H)$ . It is believed that the variation of the multidomain configuration during the magnetization reversal process with the  $\text{MR}(H) = -\text{MR}(-H)$  anomaly contributes to antisymmetric MR [56–58]. However, there are mixed reports regarding the experimental conditions required for the observation of antisymmetric MR [56–58]. Cheng *et al.* [56] observed the antisymmetric MR in Pt/Co multilayers and attributed it to the specific configuration of the mutually perpendicular direction of the domain wall, the current, and the magnetization. In contrast, Xiang *et al.* [57] observe the antisymmetric MR only when the field and current were parallel to each other. It is noteworthy that we observed antisymmetric MR only at  $T_{\text{comp}}$  (125 K) where we found highly correlated magnetic domains in the middle part of each Gd layer, using spin-dependent off-specular PNR. We believe the evolution of these highly correlated magnetic domains (with an increase in  $\sigma_m$ ) at  $T_{\text{comp}}$ , where magnetization is aligned perpendicular to the  $H$ , is responsible for antisymmetric MR. The antisymmetric MR can be explained qualitatively in line with Ref. [56] as an increase in magnetic roughness (inhomogeneities) at  $T_{\text{comp}}$  which will perturb the current propagation (electric field) and the electric field will be reversed upon magnetization reversal. However, the variation of helical magnetization as a function of temperature may contribute towards the additional irreversibility in MR across  $T_{\text{comp}}$ .

In summary, we have observed a negative exchange bias in Gd/Co multilayers below the compensation temperature ( $T_{\text{comp}} = 125 \text{ K}$ ), which increases with a decrease in

temperature. The exchange bias is due to the formation of planar domain walls across the thickness of the multilayer. Specular PNR provided the detailed depth-dependent magnetic structure of multilayers at different temperatures and suggested the formation of planar  $2\pi$  DWs, both within the Co and Gd layers at  $T_{\text{comp}}$ . PNR measurements also revealed the formation of twisted helices across  $T_{\text{comp}}$  as a result of strong exchange coupling at the interfaces. Spin-dependent off-specular PNR demonstrated the evolution of magnetic inhomogeneities (increase in magnetic roughness) and magnetic domains of size  $0.17 \mu\text{m}$  with the magnetization direction perpendicular (but in the plane) to the  $H$  in the central part of the Gd layer at  $T_{\text{comp}}$ , which are highly correlated along the thickness. These inhomogeneities and magnetic domains are responsible for antisymmetric longitudinal MR observed in Gd/Co multilayers at  $T_{\text{comp}}$ . RE-TM multilayers as artificial ferrimagnets can thus be a promising building block in devices

with all-spin-based technology due to their helical magnetic structure and the formation of planar  $2\pi$  DWs near the compensation temperature.

#### ACKNOWLEDGMENTS

The authors acknowledge the help of Nidhi Pandey and Prabhat Kumar of UGC-DAE-CSR Indore Centre during deposition of the films. We thank the ISIS Neutron and Muon source for the provision of beamtime [59]. Y.K. would like to acknowledge the Department of Science and Technology (DST), India for financial support via the DST INSPIRE Faculty research grant (DST/INSPIRE/04/2015/002938). C. L.P. thanks the DST, India (SR/NM/Z-07/2015) for the financial support for performing the experiment and Jawaharlal Nehru Centre for Advanced Scientific Research (JNCASR) for managing the project (SR/NM/Z-07/2015).

- 
- [1] I. M. Miron, K. Garello, G. Gaudin, P. J. Zermatten, M. V. Costache, S. Auffret, S. Bandiera, B. Rodmacq, A. Schuhl, and P. Gambardella, *Nature (London)* **476**, 189 (2011).
- [2] V. E. Demidov, S. Urazhdin, H. Ulrichs, V. Tiberkevich, A. Slavin, D. Baither, G. Schmitz, and S. O. Demokritov, *Nat. Mater.* **11**, 1028 (2012).
- [3] L. Q. Liu, C.-F. Pai, D. C. Ralph, and R. A. Buhrman, *Phys. Rev. Lett.* **109**, 186602 (2012).
- [4] K. S. Ryu, L. Thomas, S. H. Yang, and S. Parkin, *Nat. Nanotechnol.* **8**, 527 (2013).
- [5] S. Emori, U. Bauer, S. M. Ahn, E. Martinez, and G. S. D. Beach, *Nat. Mater.* **12**, 611 (2013).
- [6] I. E. Dzialoshinskii, *Zh. Eksp. Teor. Fiz.* **32**, 1547 (1957) [*Sov. Phys. - JETP* **5**, 1259 (1957)].
- [7] Y. K. Kato, R. C. Myers, A. C. Gossard, and D. D. Awschalom, *Science* **306**, 1910 (2004).
- [8] S. O. Valenzuela and M. Tinkham, *Nature (London)* **442**, 176 (2006).
- [9] T. Kimura, Y. Otani, T. Sato, S. Takahashi, and S. Maekawa, *Phys. Rev. Lett.* **98**, 156601 (2007).
- [10] S. H. Yang, K. S. Ryu, and S. Parkin, *Nat. Nanotechnol.* **10**, 221 (2015).
- [11] S. H. Yang and S. Parkin, *J. Phys.: Condens. Matter* **29**, 303001 (2017).
- [12] J. Finley and L. Q. Liu, *Phys. Rev. Appl.* **6**, 054001 (2016).
- [13] R. Mishra, J. Yu, X. Qiu, M. Motapothula, T. Venkatesan, and H. Yang, *Phys. Rev. Lett.* **118**, 167201 (2017).
- [14] S. A. Siddiqui, J. Han, J. T. Finley, C. A. Ross, and L. Liu, *Phys. Rev. Lett.* **121**, 057701 (2018).
- [15] X. Qiu, Z. Shi, W. Fan, S. Zhou, and H. Yang, *Adv. Mater.* **30**, 1705699 (2018).
- [16] K. J. Kim, S. K. Kim, Y. Hirata, S. H. Oh, T. Tono, D. H. Kim, T. Okuno, W. S. Ham, S. Kim, G. Go, Y. Tserkovnyak, A. Tsukamoto, T. Moriyama, K. J. Lee, and T. Ono, *Nat. Mater.* **16**, 1187 (2017).
- [17] D. Bang, J. Yu, X. Qiu, Y. Wang, H. Awano, A. Manchon, and H. Yang, *Phys. Rev. B* **93**, 174424 (2016).
- [18] R. Bläsing, T. Ma, S.-H. Yang, C. Garg, F. K. Dejene, A. T. N'Diaye, G. Chen, K. Liu, and S. S. P. Parkin, *Nat. Commun.* **9**, 4984 (2018).
- [19] T. H. Pham, J. Vogel, J. Sampaio, M. Vanatka, J.-C. Rojas-Sanchez, M. Bonfim, D. S. Chaves, F. Choueikani, P. Ohresser, E. Otero, A. Thiaville, and S. Pizzini, *Europhys. Lett.* **113**, 67001 (2016).
- [20] S. Mangin, M. Gottwald, C.-H. Lambert, D. Steil, V. Uhlir, L. Pang, M. Hehn, S. Alebrand, M. Cinchetti, G. Malinowski, Y. Fainman, M. Aeschlimann, and E. E. Fullerton, *Nat. Mater.* **13**, 286 (2014).
- [21] E. Y. Vedmedenko and D. Altwein, *Phys. Rev. Lett.* **112**, 017206 (2014).
- [22] L. V. Dzemyantsova, G. Meier, and R. Röhlberger, *Sci. Rep.* **5**, 16153 (2015).
- [23] S. Fust, S. Mukherjee, N. Paul, J. Stahn, W. Kreuzpaintner, P. Böni, and A. Paul, *Sci. Rep.* **6**, 33986 (2016).
- [24] M. R. Fitzsimmons and C. Majkrzak, in *Modern Techniques for Characterizing Magnetic Materials*, edited by Y. Zhu (Springer, New York, 2005), Chap. 3, pp. 107–155.
- [25] S. Singh, M. Swain, and S. Basu, *Prog. Mater. Sci.* **96**, 1 (2018).
- [26] S. Singh, M. R. Fitzsimmons, T. Lookman, J. D. Thompson, H. Jeon, A. Biswas, M. A. Roldan, and M. Varela, *Phys. Rev. Lett.* **108**, 077207 (2012).
- [27] S. Singh, S. Basu, M. Gupta, C. F. Majkrzak, and P. A. Kienzle, *Phys. Rev. B* **81**, 235413 (2010).
- [28] S. Singh, C. L. Prajapat, D. Bhattacharya, S. K. Ghosh, M. R. Gonal, and S. Basu, *RSC Adv.* **6**, 34641 (2016).
- [29] A. Tayal, M. Gupta, A. Gupta, V. Ganesan, L. Behera, S. Singh, and S. Basu, *Surf. Coat. Technol.* **275**, 264 (2015).
- [30] See Supplemental Material at <http://link.aps.org/supplemental/10.1103/PhysRevB.100.140405> for the basic PNR technique in the specular and off-specular mode as well as XRR and PNR data analysis and explanations of the MR data.
- [31] J. P. Andrés, L. Chico, J. Colino, and J. M. Riveiro, *Phys. Rev. B* **66**, 094424 (2002).
- [32] J. P. Andrés, J. A. González, T. P. A. Hase, B. K. Tanner, and J. M. Riveiro, *Phys. Rev. B* **77**, 144407 (2008).
- [33] JCPDS card No: 72-2223.
- [34] M. A. Basha, C. L. Prajapat, M. Gupta, H. Bhatt, Y. Kumar, S. K. Ghosh, V. Karki, S. Basu, and S. Singh, *Phys. Chem. Chem. Phys.* **20**, 21580 (2018).

- [35] S. Singh and S. Basu, in *DAE Solid State Physics Symposium*, edited by R. Chitra, S. Bhattacharya, and N. K. Sahoo, AIP Conf. Proc. (AIP, Melville, NY, 2016), Vol. 1731, p. 080007.
- [36] L. G. Parratt, *Phys. Rev.* **95**, 359 (1954).
- [37] W. H. Press *et al.*, *Numerical Recipes in Fortran: The Art of Scientific Computation*, 2nd ed. (Cambridge University Press, Cambridge, U.K., 1992).
- [38] I. Bakonyi, E. Simon, B. G. Tóth, L. Péter, and L. F. Kiss, *Phys. Rev. B* **79**, 174421 (2009).
- [39] D. D. Sarma, S. Ray, K. Tanaka, M. Kobayashi, A. Fujimori, P. Sanyal, H. R. Krishnamurthy, and C. Dasgupta, *Phys. Rev. Lett.* **98**, 157205 (2007).
- [40] S. Jana, S. Middey, and S. Roy, *J. Phys.: Condens. Matter* **22**, 346004 (2010).
- [41] Y. Kamiguchi, Y. Hayakawa, and H. Fujimori, *Appl. Phys. Lett.* **55**, 1918 (1989).
- [42] H. Fujimori, Y. Kamiguchi, and Y. Hayakawa, *J. Appl. Phys.* **67**, 5716 (1990).
- [43] M. Vaezzadeh, B. George, and G. Marchal, *Phys. Rev. B* **50**, 6113 (1994).
- [44] J. Colino, J. P. Andrés, J. M. Riveiro, J. L. Martínez, C. Prieto, and J. L. Sacedón, *Phys. Rev. B* **60**, 6678 (1999).
- [45] S. J. Blundell and J. A. C. Bland, *Phys. Rev. B* **46**, 3391 (1992).
- [46] A. Rühm, B. P. Toperverg, and H. Dosch, *Phys. Rev. B* **60**, 16073 (1999).
- [47] B. P. Toperverg, *Appl. Phys. A* **74**, s1560 (2002).
- [48] J. F. Lynn and P. A. Seeger, *At. Data Nucl. Data Tables* **44**, 191 (1990).
- [49] R. E. Camley and R. L. Stamps, *J. Phys.: Condens. Matter* **5**, 3727 (1993).
- [50] S. K. Sinha, E. B. Sirota, S. Garoff, and H. B. Stanley, *Phys. Rev. B* **38**, 2297 (1988).
- [51] V. Lauter-Pasyuk, H. J. Lauter, B. P. Toperverg, L. Romashev, and V. Ustinov, *Phys. Rev. Lett.* **89**, 167203 (2002).
- [52] B. Nickel, A. Rühm, W. Donner, J. Major, H. Dosch, A. Schreyer, H. Zabel, and H. Humblot, *Rev. Sci. Instrum.* **72**, 163 (2001).
- [53] F. Canet, C. Bellouard, S. Mangin, C. Chatelain, C. Senet, R. Siebrecht, V. Leiner, and M. Piecuch, *Eur. Phys. J. B* **34**, 381 (2003).
- [54] A. Paul, S. Mukherjee, W. Kreuzpaintner, and P. Böni, *Phys. Rev. B* **89**, 144415 (2014).
- [55] S. Mangin, T. Hauet, Y. Henry, F. Montaigne, and E. E. Fullerton, *Phys. Rev. B* **74**, 024414 (2006).
- [56] X. M. Cheng, S. Urazhdin, O. Tchernyshyov, C. L. Chien, V. I. Nikitenko, A. J. Shapiro, and R. D. Shull, *Phys. Rev. Lett.* **94**, 017203 (2005).
- [57] G. Xiang, A. W. Holleitner, B. L. Sheu, F. M. Mendoza, O. Maksimov, M. B. Stone, P. Schiffer, D. D. Awschalom, and N. Samarth, *Phys. Rev. B* **71**, 241307(R) (2005).
- [58] W. Desrat, S. Kamara, F. Terki, S. Charar, J. Sadowski, and D. K. Maude, *Semicond. Sci. Technol.* **24**, 065011 (2009).
- [59] RB1768003 and OFFSPEC data, doi:10.5286/ISIS.E.92918790.